The Astrophysical Journal Letters, 969:L31 (9pp), 2024 July 10 https://doi.org/10.3847/2041-8213/ad5a95

From Seeds to Supermassive Black Holes: Capture, Growth, Migration, and Pairing in Dense Protobulge Environments

Yanlong Shi[1,2], Kyle Kremer[1], and Philip F. Hopkins[1]
[1] TAPIR, MC 350-17, California Institute of Technology, Pasadena, CA 91125, USA; yanlong.astro@outlook.com
[2] Canadian Institute for Theoretical Astrophysics, University of Toronto, Toronto, ON M5S 3H8, Canada
Received 2024 June 2; revised 2024 June 16; accepted 2024 June 16; published 2024 July 8

Abstract

The origins and mergers of supermassive black holes (SMBHs) remain a mystery. We describe a scenario from a novel multiphysics simulation featuring rapid ($\lesssim$1 Myr) hyper-Eddington gas capture by a $\sim$1000 $M_\odot$ "seed" black hole (BH) up to supermassive ($\gtrsim 10^6\,M_\odot$) masses in a massive, dense molecular cloud complex typical of high-redshift starbursts. Due to the high cloud density, stellar feedback is inefficient, and most of the gas turns into stars in star clusters that rapidly merge hierarchically, creating deep potential wells. Relatively low-mass BH seeds at random positions can be "captured" by merging subclusters and migrate to the center in $\sim$1 freefall time (vastly faster than dynamical friction). This also efficiently produces a paired BH binary with $\sim$0.1 pc separation. The centrally concentrated stellar density profile (akin to a "protobulge") allows the cluster as a whole to capture and retain gas and build up a large (parsec-scale) circumbinary accretion disk with gas coherently funneled to the central BH (even when the BH radius of influence is small). The disk is "hypermagnetized" and "flux-frozen": dominated by a toroidal magnetic field with plasma $\beta \sim 10^{-3}$, with the fields amplified by flux-freezing. This drives hyper-Eddington inflow rates $\gtrsim 1\,M_\odot\,\mathrm{yr}^{-1}$, which also drive the two BHs to nearly equal masses. The late-stage system appears remarkably similar to recently observed high-redshift "little red dots." This scenario can provide an explanation for rapid SMBH formation, growth, and mergers in high-redshift galaxies.

Unified Astronomy Thesaurus concepts: Accretion (14); Black hole physics (159); Intermediate-mass black holes (816); Giant molecular clouds (653); Star formation (1569)

1. Introduction

Observations of high-redshift ($z \gtrsim 7$, $\sim$0.7 Gyr since the Big Bang) quasars demonstrate the existence of supermassive black holes (SMBHs) of $>10^9\,M_\odot$ at these very early stages of the Universe (Fan et al. 2001; Yang et al. 2020; Wang et al. 2021). How SMBHs form at all—let alone how they grow so quickly—remains a major unsolved problem (Inayoshi et al. 2020; Volonteri et al. 2021). Evidence from low-redshift studies argues that such SMBHs grow from "seed" masses (perhaps even as low as stellar 10–100 $M_\odot$) via gas accretion (Yu & Tremaine 2002). But assuming accretion is radiatively inefficient (and spherical), the Eddington limit is commonly cited as setting a classical upper limit to the black hole (BH) accretion rate, which is defined as $\dot{M}_{\rm Edd} = M_{\rm BH}/(\epsilon_{\rm ref}\,t_{\rm Sal})$, where $t_{\rm Sal} = \kappa_{\rm es}c/(4\pi G) \approx 45$ Myr is the Salpeter time and $\epsilon_{\rm ref}$ is an assumed radiative efficiency (typically 0.1; Inayoshi et al. 2020). Thus, to grow to SMBH masses from "seed" masses $\ll 10^6\,M_\odot$ (Greene et al. 2020) at high redshifts generally requires either accretion well above this naive Eddington limit (Inayoshi et al. 2016; Shi et al. 2023) or exotic intermediate-mass black hole (IMBH) seed formation scenarios like the direct collapse of unfragmented giant molecular clouds (GMCs) to single hypermassive stars (with SMBH masses themselves; Bromm & Loeb 2003), exotic dark matter/new physics processes (Xiao et al. 2021), or runaway mergers of stars (Portegies Zwart et al. 2004; Shi et al. 2021; Rantala et al. 2024).

Theoretical work on small-scale ($\sim$au or horizon-scale) accretion physics has shown that super-Eddington accretion is possible (Begelman 1979; Blandford & Begelman 2004; Inayoshi et al. 2016). This is primarily enabled by the "photon trapping" effect, in which photons are trapped in the strong accretion flow ($\sim 1000\dot{M}_{\rm Edd}$) and advected into the BH (radiating inefficiently). This is also demonstrated by numerical simulations (Jiang et al. 2014, 2019; Sądowski et al. 2015), where a sustainable phase of super-Eddington accretion is observed. But these simulations focus only on the accretion disk scales well interior to radii where the BH dominates the potential: another (perhaps more challenging) requirement for super-Eddington accretion is that the BH can gravitationally capture sufficient gas (from its turbulent, star-forming interstellar medium, ISM, environment) to sustain such accretion for the time needed to grow. This could be especially challenging in high-redshift galaxies where star formation is clumpy and bursty, potentially scattering BH seeds and inhibiting large-scale, coherent accretion flows (Ma et al. 2021; Byrne et al. 2023). Furthermore, classical accretion disk models (Shakura & Sunyaev 1973) predict that such a super-Eddington accretion disk should be violently gravitationally unstable and fragment outside of tens of gravitational radii ($GM_{\rm BH}/c^2$) from the horizon (Goodman 2003).

Some of the problems above are explored in Shi et al. (2023), where we embedded BH seeds into star-forming GMCs. We found that significant BH accretion can "stochastically" occur if a dense clump (parsec or subparsec scale) formed via turbulence and stellar feedback shocks (Klessen 2000; Mac Low & Klessen 2004; McKee & Ostriker 2007) is sufficiently gravitationally bound and close (subparsec) to the BH and if the gas is sufficiently dense and cold (Inayoshi et al. 2016). In practice, this "clump accretion" only occurs if

both the gas and the BH dynamics are dominated by the GMC's self-gravity, and stellar feedback is globally inefficient (unable to rapidly unbind all the gas in the GMC as soon as the first massive stars form; Shi et al. 2023), which is true for GMCs with high initial surface density (Grudić et al. 2018b, 2021a; Chevance et al. 2023). In Shi et al. (2024), we extended these to include physically motivated feedback from BH accretion in the forms of radiation (Jiang et al. 2019), accretion disk winds and jets (Silk & Rees 1998; Blandford & Begelman 1999), and cosmic rays (Guo & Oh 2008; Guo & Mathews 2012; Zweibel 2017). We showed that for reasonable feedback parameters, BHs can still grow rapidly, and their growth is primarily "fueling-limited" until they reach supermassive masses and the "feedback-limited" regime. But this alone does not address many of the key questions above.

Meanwhile, in a series of papers using a different numerical method, physics, and technical approach, Hopkins et al. (2024a, 2024b) followed gas accreting onto a preexisting SMBH from cosmological initial conditions including star formation and found a novel type of BH accretion disk: one that is "hypermagnetized" (ratio of thermal to magnetic pressure $\beta \ll 10^{-2}$) and "flux-frozen" (dominated by a primarily toroidal magnetic field amplified from typical ISM fields by flux-freezing). In these papers and a subsequent analytic study (Hopkins et al. 2024c), they showed that these disks could resolve a number of problems posed by classic accretion disk models (like Shakura & Sunyaev 1973) that assume $\beta \gg 1$, most notably that the disk can remain stable (with Toomre $Q \gg 1$) out to $\gtrsim$parsec scales even with accretion rates thousands of times larger than the nominal Eddington limit.

Here, we present a case study of one of the massive, high-density cloud-complex simulations in Shi et al. (2023, 2024), representative of plausible starburst conditions in high-redshift progenitors of massive galaxies. We show that this demonstrates a number of remarkable phenomena that could unify many previously proposed mechanisms to enable rapid formation of a well-defined dynamical center, "trapping" of BHs, efficient and rapid migration of BH pairs to the center, efficient gas capture, and hyper-Eddington accretion through a hypermagnetized accretion disk. We show this is able to take a BH from "seed" masses to truly supermassive masses in less than 1 Myr, providing a natural theoretical scenario for high-redshift BH growth.

2. Simulation

The simulation is one of the suite in Shi et al. (2024), where the numerics are described in detail, so we only briefly summarize the salient properties here. We utilize the magnetohydrodynamics (MHD) code GIZMO[3] with MHD solved using the meshless finite mass method (Hopkins 2015; Hopkins & Raives 2016) and self-gravity using a tree-particle mesh method with self-consistent adaptive force softenings (Hopkins et al. 2023). In addition to self-gravity and (ideal) MHD, the code includes radiative cooling and heating, star formation, and stellar feedback, following the treatments in Grudić et al. (2018b) and Shi et al. (2021, 2023, 2024). In detail, stars form from gas that is dense, molecular, rapidly cooling, and Jeans-unstable below the resolution limit, and stars subsequently influence the medium via five-band (far-UV through IR) radiation (heating and photon momentum), stellar mass loss, and supernovae, with rates tabulated assuming a well-sampled universal stellar initial mass function (IMF) per the FIRE-2 implementation (Hopkins et al. 2018a, 2018b) of the Feedback In Realistic Environments (FIRE) physics (Hopkins et al. 2014). Previous studies have shown that this predicts reasonable properties of star formation, molecular clouds, and star clusters on galactic (Orr et al. 2018; Benincasa et al. 2020; Keating et al. 2020; Orr et al. 2020, 2021) and individual star cluster (Grudić et al. 2018a, 2018b, 2021b, 2023; Guszejnov et al. 2020; Bruel et al. 2023; Rodriguez et al. 2023) scales.

In order to achieve a controlled experiment, we consider a noncosmological idealized experiment of an initially turbulent, magnetized cloud complex with some initial BH seed population. The complex has an initial mass of $10^8\,M_\odot$ (all gas) and a spherical radius of 50 pc, so a surface density of $\Sigma_{\rm gas} \sim 10^4\,M_\odot\,{\rm yr}^{-1}$, with an initial turbulent virial parameter of unity (and initial turbulent/zero mean magnetic fields with magnetic energy equal to 1% of gravitational energy), chosen to be representative of extreme but well-known conditions in starburst galaxy nuclei or high-redshift star-forming gas clumps in massive galaxies (Swinbank et al. 2012; Izumi et al. 2016; Scoville et al. 2017; Tacconi et al. 2018). We randomly distribute BH seeds spatially throughout the cloud, with initial masses uniformly distributed in $2 < \log_{10}(M_{\rm seed}/M_\odot) < 4$ and isotropic random velocities with the cloud virial velocity dispersion. Once the simulation begins, seeds can capture gas that is strictly bound to the BH (including thermal, magnetic, and kinetic energies) interior to the BH sink radius (Bate et al. 1995; Shi et al. 2023), which here is $\sim$0.1 pc (sufficient to easily resolve the Bondi radius of the relevant gas for accretion even at warm molecular temperatures and the tidal radius of clumps/cores to the BHs, though of course much larger than the BH gravitational radii), comparable to state-of-the-art "hyperresolution" simulations from ISM/galaxy scales (Anglés-Alcázar et al. 2021). Since this still leaves the inner accretion disk unresolved, we use a subgrid model (for a detailed description, see Shi et al. 2024) to approximate the rate of this captured gas accreting onto the BH's inner disk ($\dot{M}_{\rm BH,0} \approx M_{\rm gas,disk}/t_{\rm dep}$) with some disk depletion time following a Shakura & Sunyaev (1973)–like scaling. Apart from the mass accretion rate $\dot{M}_{\rm BH}$ that eventually contributes to the BH's mass growth, some mass $\dot{M}_{\rm w} = \eta_{\rm w}\dot{M}_{\rm BH} = \eta_{\rm w}/(1+\eta_{\rm w})\dot{M}_{\rm BH,0}$ is assumed to be ejected in winds and bipolar jets following the methods in Torrey et al. (2020) and Su et al. (2021) with effective large-scale (emergent from unresolved sales) velocity $v_{\rm j}$, while a fraction $\epsilon_{\rm r}$ emerges as radiation with the Shen et al. (2020) template spectrum. We set $\eta_{\rm w} = 1$, $v_{\rm j} = 400\,{\rm km\,s^{-1}}$, $\epsilon_{\rm r} = 10^{-5}$. These are chosen to be representative of properties of super-Eddington "slim disk" models accreting at the hyper-Eddington rates we will find (Watarai et al. 2000; Jiang et al. 2019), but a parameter study of the effects of these choices is the subject of Shi et al. (2024). We run the simulation for 1.8 Myr (a few times the initial global complex freefall time), at which point we show that the system is in a quasi-steady state, with most star formation and BH growth complete.

To build a star subcluster merger history in postprocessing, we first identify gravitationally bound star clusters in each snapshot.[4] To check the inheritance relationship between

[3] http://www.tapir.caltech.edu/~phopkins/Site/GIZMO.html

[4] https://github.com/mikegrudic/Phinder

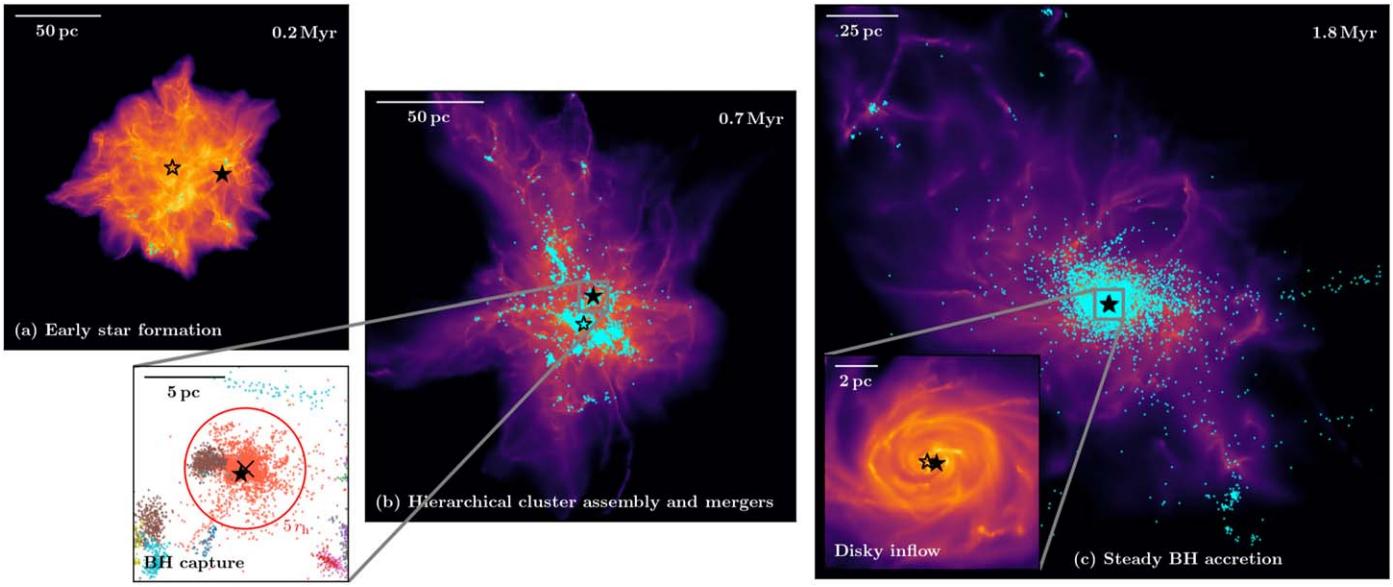

Figure 1. Visualization of the simulation. We show the gas morphology (column density in logarithmic scales) and positions of star particles (colored dots; only a subset is displayed for esthetic purposes) and two selected BHs (black stars) at different stages of the simulation. Panel (a): early star formation ($t \ll t_{\rm ff}$), where seed BHs wander in the GMC. Panel (b): hierarchical cluster assembly and mergers ($t \sim t_{\rm ff}$), where bursty star formation happens but the GMC is bound due to strong self-gravity. Massive subclusters form, and one of the BHs is "captured" by (gravitationally bound to) a cluster (red dots in the inserted zoom-in panel, where the radius of the red circle equals five half-mass radii of the cluster). Panel (c): protobulge formation and steady BH accretion ($t \gtrsim 2\ t_{\rm ff}$), where subclusters merge into the final massive cluster, and the seed BH captured by the subcluster is migrated to the center. The inserted zoom-in panel shows the gas morphology around the BHs, which suggests convergent inflow and disk structure.

cluster i in one snapshot and cluster j in another one, we use a "similarity measure," which is defined as $s_{ij} = [n_{ij}/\min(n_i, n_j)] \cdot [2\sqrt{n_i n_j}/(n_i + n_j)]$, where n_i (n_j) is the number of particles in the cluster i (j) and n_{ij} is the number of common particles between the two clusters. For a cluster in one snapshot, we iterate over clusters in the next snapshot to rank and determine the most possible successor (above a preset threshold). A "merger tree" is constructed after iterating over all clusters and all snapshots (densely sampling the local dynamical times) in the simulation.

3. Protobulge Formation and BH Capture and Migration

Figure 1 shows the gas and stellar morphology at different evolution stages in the simulation. The simulation starts with a smooth density profile with initial turbulence seeded. Then gravitational collapse occurs, and the medium becomes more turbulent, creating dense clumps, shocks, and filaments. Star formation begins in these dense regions well before one global freefall time. The high surface density (or, equivalently, "gravitational pressure" or acceleration) scale is critical: it means the gas is not fully disrupted by "early" (presupernova) stellar feedback, despite turning most of its initial gas mass into stars, owing to the strong self-gravity. That in turn means that the bound-cluster star formation efficiency in the various subclumps is large (i.e., we form dense, bound subclusters and not an unbound, low-density open cluster/association), consistent with both analytic expectations and results from a wide variety of simulations (Wada et al. 2009; Fall et al. 2010; Hopkins et al. 2016, 2022; Grudić et al. 2019, 2020).

Given the high star formation efficiency, we see these form into hierarchical subclusters that merge rapidly, as in local young massive clusters (Grudić et al. 2018a; Li et al. 2019; Guszejnov et al. 2022). In Figure 2, we show the trajectories of (sub)cluster centers, following their merger history. We can see that clusters merge rapidly after their formation and migrate to the center. We also plot the trajectories of the two BH seeds with the most significant mass accretion (same as those in Figure 1) and highlight cluster merger tracks that interact with them. BH 1 encounters cluster merger track 1 at ∼0.4 Myr and becomes captured by that cluster; it then oscillates along the cluster's trajectory before settling down in the cluster. The BH–cluster pair then migrate to the center at ∼1.1 Myr. A similar process occurs for the second BH–cluster pair, though this capture happens at ∼0.7 Myr and is much closer to the center. These two clusters later merge at ∼1.1 Myr, rapidly bringing the BHs together to form a binary. We do not allow the BHs to merge since we do not resolve the radii ($\ll$0.1 pc) where gravitational-wave emission would become important to coalescence.

The merger history of clusters is also reflected in their mass evolution, as shown in the top right panel of Figure 2. The two clusters merge into a very massive cluster ($\sim 4 \times 10^7\,M_\odot$) at ∼1 Myr, after which the clusters' mass growth stalls. We also plot the mass evolution of the two BHs that grow most effectively. Both BHs reach $\sim 10^4\,M_\odot$ by ∼0.5 Myr, with most of this "early" accretion occurring when a dense clump becomes gravitationally captured by the BH, similar to the behavior described in Shi et al. (2023). Note that this early "stochastic" growth is shown in Shi et al. (2023) to be essentially independent of seed mass over the range $M_{\rm seed} \sim 100$–$10^4\,M_\odot$, consistent with what we see here (where one seed has about the median mass of our random seeding, while the other happens to be toward the high-mass end of our initial seed spectrum). What is more important is that these seeds (of the ∼100 initial seeds placed randomly throughout the complex) happened to be at the "right place at the right time" to be captured and reach the center of their subcluster quickly. After ∼0.75 Myr, the two BHs have reached the cluster center and the cluster has started to coalesce and relax,

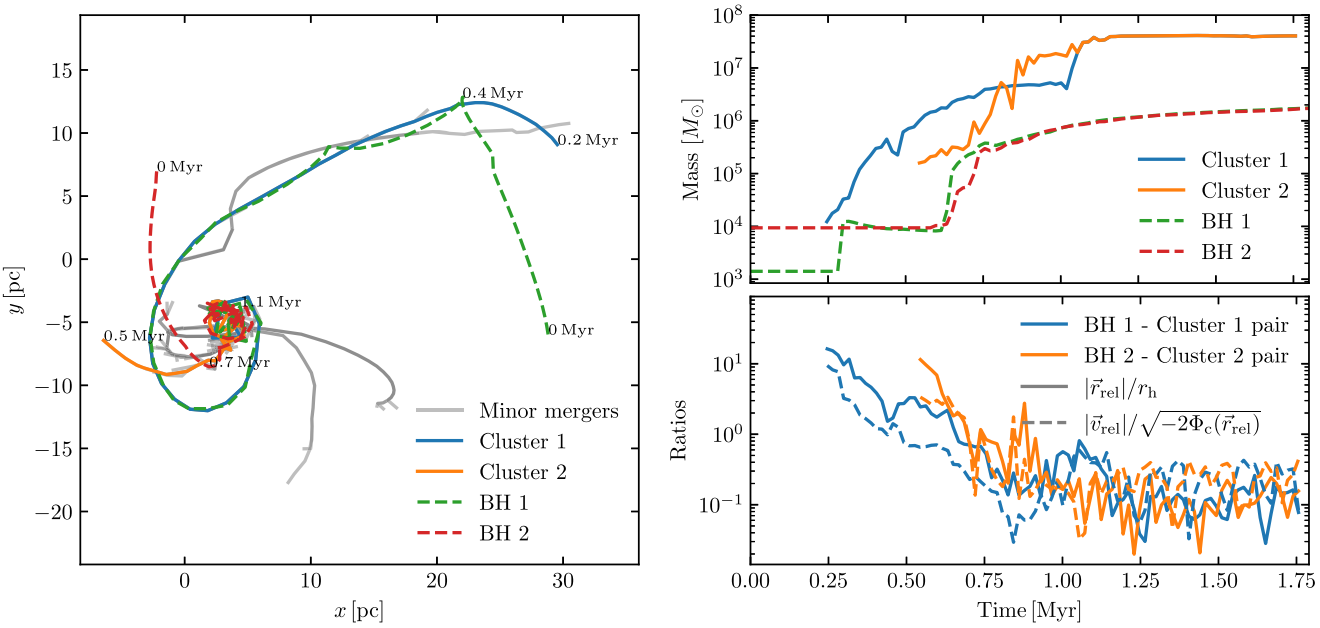

Figure 2. BH capture, migration, and growth as subclusters merge. Left: trajectories of the centers of mass of the two subclusters (1, 2; solid), which capture the two BHs (1, 2; dashed) from Figure 1. The BHs are "captured" (become bound to the subcluster) at the times labeled, well before they reach the center, and are carried to the center by the merging subclusters. Minor subclusters merged into these two massive clusters are tracked with gray lines. Top right: mass evolution of the subclusters and BHs. Clusters acquire mass initially through star formation and then hierarchical merging, which completes (and the system relaxes) by ∼1 Myr. The BHs grow in early "jumps" as they accrete clumps near their subcluster centers and then at a steady rate ∼1–5 $M_\odot$ yr^{-1} after ∼0.7 Myr from the nuclear disk. Bottom right: boundedness/sinking of each BH in its subcluster. We show the spatial ($|\boldsymbol{r}_{\rm rel}|$; solid) and velocity ($|\boldsymbol{v}_{\rm rel}|$; dashed) separation between the BH and its subcluster center of mass, normalized by the subcluster half-mass radius $r_{\rm h}$ or escape velocity $\sqrt{-2\Phi_{\rm c}(\boldsymbol{r}_{\rm rel})}$. The BHs sink and become more confined as their subclusters grow and merge.

so the large-scale accretion flow (discussed below) becomes more stable and the BHs continue to grow almost linearly in time, i.e., at a constant $\dot{M}_{\rm BH} \sim 2-5\,M_\odot$ yr^{-1}. They finally both reach $\sim 2\times10^6\,M_\odot$ at the end of the simulation. Note that at all times, the BHs are much less massive than their host (sub) cluster, so their large-scale sinking and coalescence to the center, over a distance of ∼50 pc, is enabled by the rapid dynamical hierarchical subcluster merging. If the BH seeds instead had to sink to the center of the final, relaxed/smooth star cluster as isolated objects (i.e., via classical dynamical friction), the dynamical friction time would be $>10^{10}$ yr. Instead, since the subclusters hierarchically merge in $\mathcal{O}(1)$ mass ratios, the BHs can be carried to the center in of order one dynamical time (Guszejnov et al. 2022, and references therein).

Through evolution, each cluster also changes its mass $M_{\rm c}$ and half-mass radius $r_{\rm h}$. For the two clusters highlighted in Figure 2, mass growth and the accompanying deepening of their potential well enhance capture of their respective BHs. This is illustrated in the bottom right panel of Figure 2, where we track the relative distance ($\boldsymbol{r}_{\rm rel}\equiv\boldsymbol{r}_{\rm BH}-\boldsymbol{r}_{\rm cluster}$, normalized to $r_{\rm h}$, where $\boldsymbol{r}_{\rm cluster}$ is the cluster's gravitational center) and velocity ($\boldsymbol{v}_{\rm rel}=d\boldsymbol{r}_{\rm rel}/dt$, normalized to the escape velocity at the BH position $v_{\rm esc}=\sqrt{-2\Phi_{\rm c}(\boldsymbol{r}_{\rm rel})}$, where we calculate the gravitational potential $\Phi_{\rm c}(\boldsymbol{r}_{\rm rel})\equiv-\sum_i Gm_i/|\boldsymbol{r}_{\rm BH}-\boldsymbol{r}_i|$ at the BH position from all stars in the cluster at that time). We see distance and velocity decay in $\lesssim$1 Myr (the same is true if we measure the specific angular momentum) for both the BHs within their subclusters and the subclusters with respect to the parent cloud/cluster. But we see that capture is not just due to a chance encounter between a BH and subcluster at low speeds (which would be rare). Rather, Figure 2 shows that the two BH–cluster pairs are not gravitationally bound initially, and indeed, the relative velocities of the BHs to clusters actually increase (from ∼50 to ∼200 km s^{-1}) from early to late times, but the ratios of kinetic to potential energy become <1, and the BHs are captured at 0.4 and 0.7 Myr, the same times that their clusters grow rapidly in mass, increasing $|\Phi_{\rm c}|$ and the subcluster escape velocity rapidly relative to the (relatively weakly evolving) $v_{\rm rel}$.

The final merged star cluster has a mass of $\sim5\times10^7\,M_\odot$ but with a dense central mass concentration (half-mass radius of ∼3 pc) and isothermal-sphere-like density profile $\rho_*\propto r^{-2}$ steepening to r^{-4} at larger radii after undergoing violent relaxation from multiple hierarchical subcluster mergers. This means that the characteristic circular velocity is large, ∼200 km s^{-1} (see Section 4), and the cluster lies in between massive typical nearby star clusters and galactic bulges in most structural and kinematic scaling relations (where the two are known to form a continuous family; see Hopkins et al. 2010; Grudić et al. 2019). Indeed, these are very similar stellar masses, sizes, surface densities, velocity dispersions, and density profiles to known massive nuclear star clusters and ultracompact dwarfs observed (Geha et al. 2002; Haşegan et al. 2005; Walcher et al. 2005; Evstigneeva et al. 2007). So, given the initial gas and final stellar properties, this suggests a picture where these "protobulges" form from sufficiently high-density gas complexes in high-redshift massive galaxy progenitors, which rapidly fragment into subclusters that can capture (even relatively modest mass) BH "seeds" and hierarchically merge in a dynamical time (as argued from some cosmological simulations in, e.g., Ma et al. 2018, 2020), forming a deep, centrally concentrated potential that traps and brings together the BHs.

It is worth mentioning that hierarchical star cluster assembly is a process with ample dynamics that may produce massive seed BHs. For example, Rantala et al. (2024) found that the

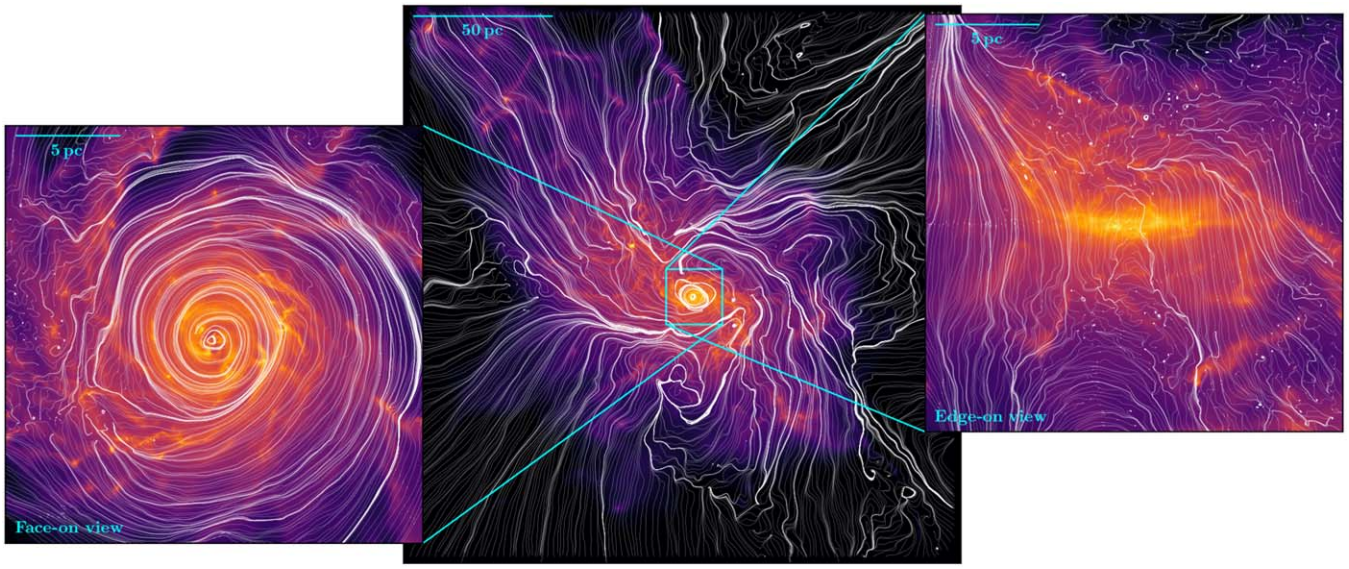

Figure 3. Magnetic field lines (near the midplane of each box) and gas morphology (logarithm of the column density) at the late stage of the simulation. The main panel suggests that the large-scale magnetic field is advected to smaller scales due to gravitational collapse throughout the simulation. The inserted zoom-in panels focus on the disk structure, adapted to face-on (left panel) and edge-on (right panel) views. The face-on view shows a dominant toroidal magnetic field spiraling inward counterclockwise, while the edge-on view shows the (weaker) poloidal magnetic field lines threading through the disk structure.

process may boost the formation of very massive stars through repeated star mergers, which can be progenitors of BH seeds. Still, for the gas-rich environments that this work is focused on, BH accretion can play an important role in the "protobulge" system. We expand on these details in the next section.

4. Sustained Hyper-Eddington Accretion through a Hypermagnetized Disk

As the clusters begin to dynamically "settle" after ∼0.4–0.7 Myr, we see an extended accretion disk appear and grow "inside out," beginning just outside the sink radius until ultimately extending to $\gtrsim$10 pc scales. Figure 1 plainly shows the disk in the last inserted panel, while Figure 3 shows the magnetic field structures. We overplot the magnetic field vectors, which are clearly dominated by a dominant mean toroidal/azimuthal field, though there are also poloidal fields vertically threading through the disk. This results in the nearly constant growth shown in Figure 2 at ∼1–10 $M_\odot\,\mathrm{yr}^{-1}$ for the remaining $\gtrsim$1 Myr. From this and the BH masses, we see that this is well above the Eddington limit, which ranges from ∼0.006 to 0.04 $M_\odot\,\mathrm{yr}^{-1}$ over the same time. We also see that the disk extends well outside the BH radius of influence (ROI),

$$R_{\rm ROI} = GM_{\rm BH}/\sigma_*^2 \sim 0.1\ \mathrm{pc}(M_{\rm BH}/10^6 M_\odot)(\sigma_*/200\ \mathrm{km\ s^{-1}})^{-2}.$$

We summarize the gas disk properties in Figure 4. We confirm both that it is indeed a disk (primarily rotation-supported with $\langle v_\phi\rangle \approx V_{\rm c}^{\rm total} = \sqrt{GM_{\rm tot}(<R)/R}$ out to $\gtrsim$10 pc) and that it clearly appears to be an example of the "hypermagnetized" or "flux-frozen" disks proposed in Hopkins et al. (2024a, 2024b, 2024c). The defining properties of these disks, all of which we see in Figure 4, are that magnetic pressure dominates in the midplane (plasma $\beta \sim P_{\rm thermal}/P_{\rm B} \sim c_s^2/v_A^2 \sim 10^{-3}$ here),[5] coming primarily from a mean toroidal field (with $\langle B_\phi\rangle$ much larger than either the mean radial/poloidal fields B_R, B_z or turbulent fields) with trans- (or weakly sub-) Alfvénic turbulence ($v_{\rm turb} \sim v_{\rm A}$ here). One can verify from Figure 4 that the accretion rates through the disk are approximately constant (∼1–10 $M_\odot\,\mathrm{yr}^{-1}$) with R, with values consistent with the measured mean radial $\langle v_R\rangle$ and Maxwell+Reynolds stresses directly extracted from the simulation (note the expected $\langle B_R\rangle - \langle B_\phi\rangle$ anticorrelation, discussed in Hopkins et al. 2024b, which ensures a strong Maxwell stress of the desired sign), as well as that the (thick) vertical height behaves as expected from magnetic+turbulent support ($H/R \sim \sigma_z/V_{\rm c} \sim v_{\rm A}/V_{\rm c} \sim 0.3$–1), and the midplane density scales accordingly ($\rho \sim \Sigma_{\rm gas}/2H$). For a detailed analysis of these properties in such disks, we refer to Hopkins et al. (2024b).

The magnetic field strengths appear to be consistent with growth via flux-freezing/advection of magnetic flux from the diffuse gas into and throughout the disk: B_ϕ rises approximately as r^{-1} from a couple hundred μG (the value of the turbulent field in the initial conditions, comparable to that observed in gas with a mean density similar to the initial cloud value $n \sim 10^4\,\mathrm{cm}^{-3}$ in the ISM; see Crutcher 2012; Ponnada et al. 2022) to ∼0.1 G on subparsec scales. If we follow the componentwise analysis in Hopkins et al. (2024b), this amplification and the $B_\phi - B_R$ anticorrelation are consistent with the mean-field Lagrangian induction equation, as the gas is captured and compressed (and the fields "wound up" toroidally) as it accretes.[6] As well, we overplot the specific analytic model dependence of $\rho(R)$, $B(R)$ from Hopkins et al. (2024c) after modifying their model to account for the non-Keplerian potential seen here (below) and see reasonable agreement.

[5] We have verified, and it is expected from simple dimensional arguments, that radiation pressure is negligible in the midplane at these (large) disk radii.

[6] We can also verify that our assumption of ideal MHD is valid. The microphysical Spitzer/Braginskii conduction/viscosity coefficients are tiny under these gas conditions (equivalently, the particle mean free paths are extremely small compared to $\sim H$). And comparing nonideal ohmic/Hall/ambipolar resistivities (e.g., Kunz & Mouschovias 2009) to the turbulent diffusivities $\sim v_t H$ shows that the microphysical nonideal terms are smaller by at least ∼5–10 orders of magnitude, owing to a combination of the relatively low gas densities and high ionization fractions $f_{\rm ion} \sim 0.01$ given the extreme stellar irradiation of the low-density disk.

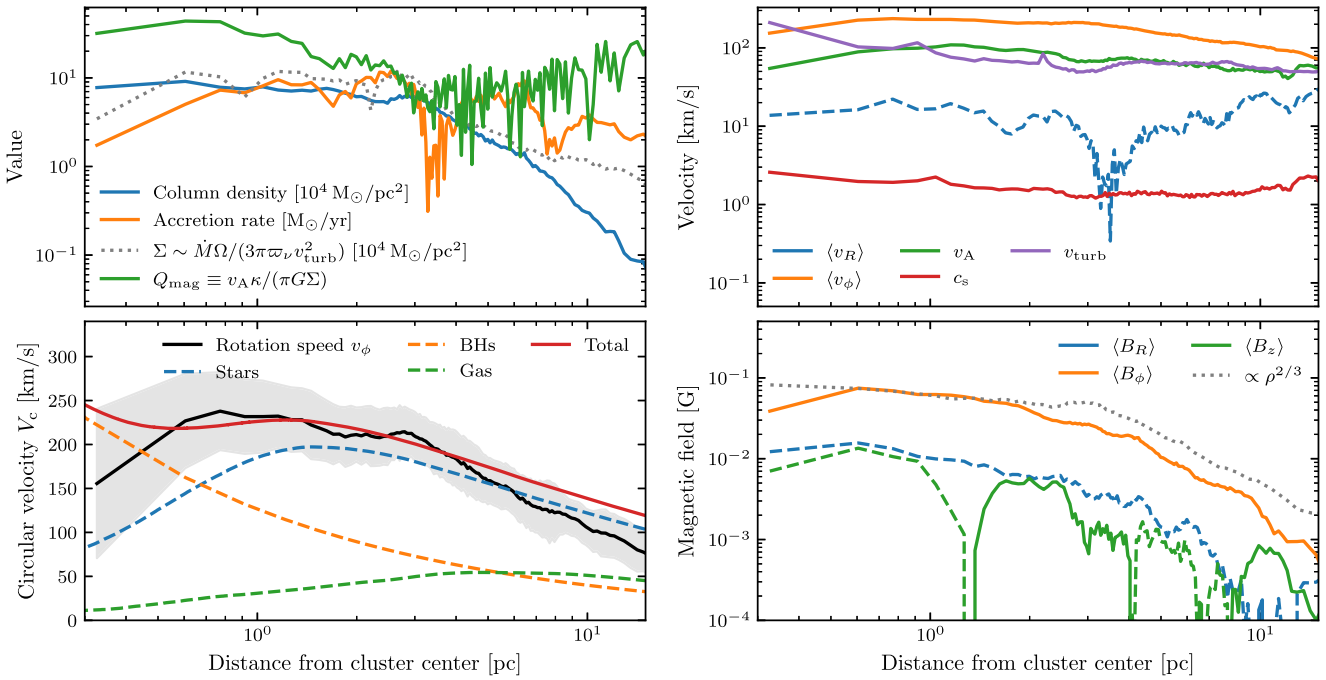

Figure 4. Dynamics and magnetic field of the disk. Upper left: surface/column density, mass accretion rate, and magnetic Toomre $Q_{\rm mag}$ profiles of the disk (measured in cylindrical annuli). We also plot the predicted surface density $\Sigma(R)$ for the analytic hypermagnetized disk models in Hopkins et al. (2024c), assuming an accretion rate $\dot{M}/\varpi_\nu = 30\,M_\odot$ yr^{-1}. Lower left: mean rotation velocity v_ϕ of the gas measured from the simulation (with the gray band representing the standard deviation), and the total circular velocity $\equiv\sqrt{G\,M_{\rm tot}(<R)/R}$ with the contribution $\equiv\sqrt{G\,M_i(<R)/R}$ the mass of stars, BHs, and gas. Upper right: average radial and azimuthal velocities (dashed if negative) of the gas in the disk and Alfvén speed ($v_{\rm A}$), thermal sound speed ($c_{\rm s}$), and rms turbulent velocities ($v_{\rm turb}$). Lower right: strength of the mean radial, toroidal, and poloidal magnetic field (dashed if negative). The overall magnetic field strength is in agreement with the flux-freezing assumption ($|\boldsymbol{B}| \propto \rho^{2/3}$; dotted).

As in Hopkins et al. (2024a), the strong magnetic field appears to stabilize the disk against fragmentation and star formation. We do not see fragmentation, and the star formation rate after the disk forms is small (Figure 2) compared to BH growth rates. Indeed, from Figure 4, we can see that the Toomre Q parameter accounting for magnetic support ($Q_{\rm mag} \equiv v_{\rm A}\kappa/\pi G\Sigma$) is $\gg$1 at all radii here (typically $\sim$20–50), while if we included only thermal pressure ($Q_{\rm therm} \equiv c_{\rm s}\kappa/\pi G\Sigma$), we would obtain $Q_{\rm therm} \sim 0.1 \ll 1$ at all radii.

The thermal properties themselves, while unimportant for the disk structure since $\beta \ll 1$ (and because we are well outside the near-horizon radii where most of the accretion disk emission originates), are reasonable. At these large ($\sim$parsec) radii, the disk self-heating flux $\sim(3/8\pi)\dot{M}\Omega^2$ is small compared to the flux from stellar irradiation. Assuming a cluster mass profile dominated by a young ($\lesssim$10 Myr) stellar population with a well-sampled IMF and standard dust composition as assumed in code, the equilibrium dust temperature (equating the stellar flux absorbed by grains to their emission) is $\sim$400 K$(V_{\rm c}/200\ {\rm km\ s^{-1}})^{2/5}(R/{\rm pc})^{-1/5}$, which at the densities here should be in rough equilibrium with the gas temperature. Indeed, this appears to reasonably predict the thermal properties in Figure 4, though we note that the disk is somewhat multiphase with a mix of warm and cool atomic, cold molecular gas and very compact H II regions around some stars.

There are some notable differences from the simulation presented in Hopkins et al. (2024a). First, the disk here forms under very different circumstances and in a very different regime of parameter space (in terms of BH mass, gas/galaxy properties, accretion rate, initial absolute magnetic field strength, etc.), and numerically, the simulations here adopt a different MHD solver, treatments of star formation and stellar feedback (FIRE versus STARFORGE; Grudić et al. 2021a), resolution, BH feedback treatment, and initial conditions. All of this argues that such disks should not be uncommon in high-accretion-rate BHs. Second, and perhaps most notably, the disk in those papers formed entirely within the ROI, where we see it extend well past the ROI here at all times. Figure 4 explicitly shows that stars dominate the potential outside $\gtrsim$0.5 pc even at the final time (when the BHs are most massive), with a somewhat flat, then again weakly declining, $V_{\rm c}(R)$. This implies that there is nothing uniquely special about a Keplerian potential required to obtain such a disk, so long as there is a well-defined centrally peaked potential and the magnetic fields, gravitational stability, and other properties of the gas permit. Indeed, we can still apply the analytic models for the predicted structure of such disks derived in Hopkins et al. (2024c) if we replace Ω in their scalings (which they took to be Keplerian) with the appropriate value here, $\Omega = V_{\rm c}/r$. If we take their default model and make this replacement, we predict $-\partial\ln B_\phi/\partial\ln R \sim 8/9 - 4/3$ and $-\partial\ln\rho/\partial\ln R \sim 4/3 - 2$ (with the shallower slopes around $\sim$0.5–3 pc, where $V_c \sim R^0$ deviates most from Keplerian), consistent with the behavior in Figure 4. This also has implications for the disk heating/thermal structure (above). Third, it is worth noting that this is formally a circumbinary disk, given the two nearly equal-mass BHs (Figure 2).

It is striking that the two BHs, once brought together at $\gtrsim$0.7 Myr, rapidly converge to nearly identical mass growth rates in the interior of the circumbinary disk. This effect has been seen before in circumbinary disk simulations (Lai & Muñoz 2023) and may explain populations of "twin stars" (El-

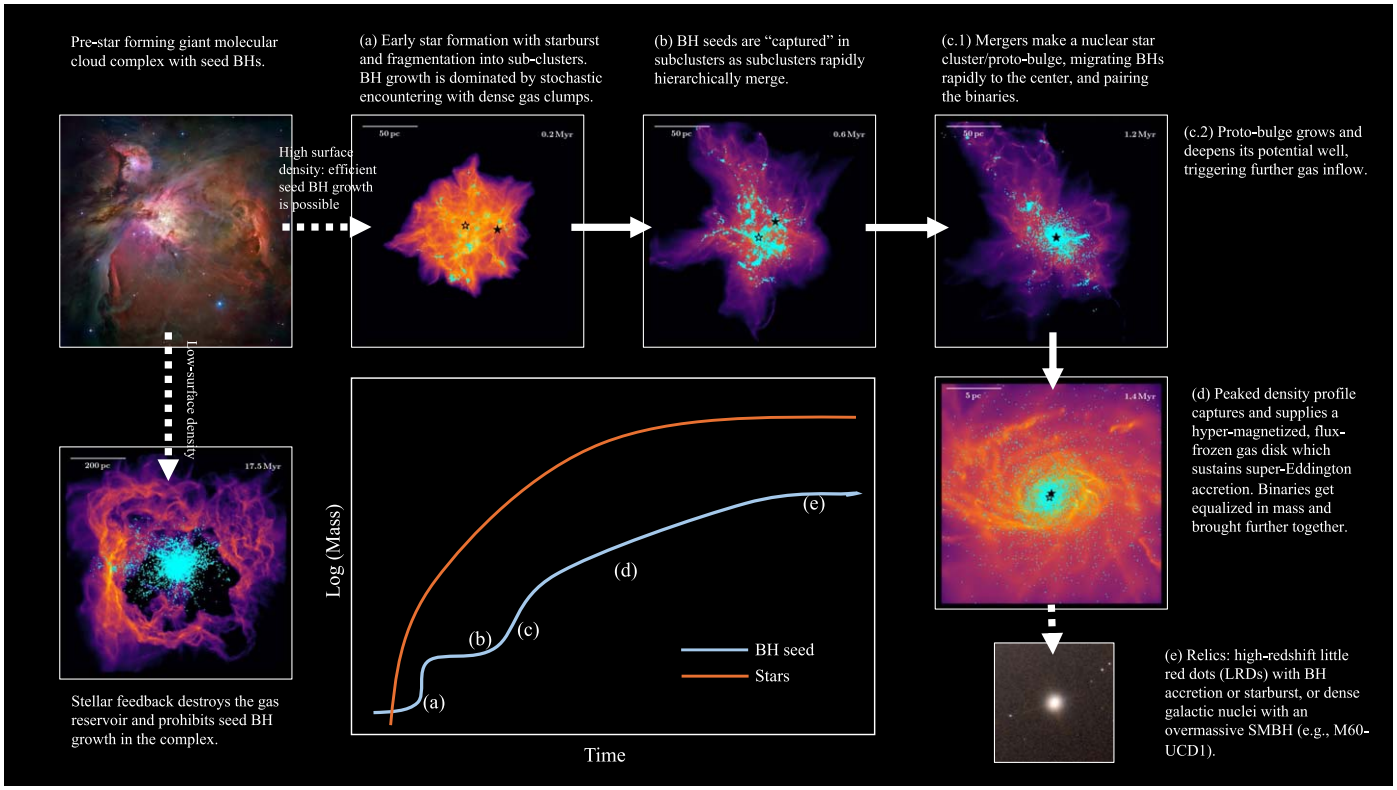

Figure 5. Illustration of the scenario of seed BH capture, growth, migration, and pairing in the star-forming GMC complex. The evolution of the star-forming complex is largely determined by the surface density, while low-surface-density clouds are expelled by stellar feedback, halting possible seed BH accretion (upper left → lower left). In high-surface-density clouds, seed BHs may undergo steps (a)–(e), corresponding to the qualitative trend of star formation and BH mass growth (lower middle panel; also see Figure 2). Image credits—M42 (upper left panel): NASA, ESA, M. Robberto (Space Telescope Science Institute/ESA) and the Hubble Space Telescope Orion Treasury Project Team; M60-UCD1 (panel (e)): NASA, ESA, and the Hubble Heritage (STScI/AURA).

Badry et al. 2019) but will clearly have important implications for BH mergers.

5. Conclusions

We present a scenario for an extremely rapid ($\sim$1 Myr) transition from seed to SMBH in a forming protobulge or massive nuclear star cluster, with efficient growth and pairing of BH binaries. This unifies many theoretical ideas that have been proposed for different aspects of the problem, demonstrating for the first time all of them operating in concert in an MHD–thermochemical–star formation simulation. Our key conclusions, which define the steps in this scenario (also see Figure 5), unfold as follows.

1. In a massive gas cloud complex of $\sim 10^8\,M_\odot$ and surface density $\Sigma \sim 10^4\,M_\odot\,\mathrm{pc}^{-2}$, typical of starburst nuclei or "clumps" in massive high-redshift galaxies, fragmentation and star formation are very efficient, and stellar feedback is weak, so many bound subclusters rapidly form. A small fraction of low-mass BH seeds can grow essentially "stochastically" to IMBH masses by encountering dense, small clumps of gas.
2. Those IMBHs are efficiently "captured" by their adjacent subclusters during this process. As the subclusters grow and merge, the BHs become even more effectively confined.
3. Subclusters merge hierarchically in essentially one dynamical time of the complex ($<$1 Myr). This builds a protobulge, with properties similar to observed massive, dense nuclear star clusters and ultracompact dwarfs, with a sharply centrally concentrated (isothermal) stellar mass profile.
4. Carried by their subclusters, the trapped BHs migrate to the center at the same time, orders of magnitude faster than their dynamical friction time if they were isolated. This also produces efficient "pairing" down to $<$1 pc scales of multiple BHs.
5. The protobulge provides a deep, centrally concentrated potential that allows gas to be globally captured and retained in the system with a coherent center and angular momentum, so it forms a large-scale accretion disk extending well beyond the BH ROI (to $\gtrsim$parsec scales). Accretion transitions from stochastic/turbulent clump–clump encounters to disk feeding.
6. As gas is captured with modest preexisting turbulent magnetic fields, the toroidal field lines are stretched and form a magnetically dominated, flux-frozen disk. The disk pressure comes from the toroidal field, with plasma $\beta \sim 10^{-3}$ in the midplane. This stabilizes the disk against catastrophic fragmentation and star formation and allows it to exist at all while simultaneously ensuring strong Maxwell and Reynolds stresses that support extremely large accretion rates of $\sim$1–10 $M_\odot\,\mathrm{yr}^{-1}$ for $\gtrsim$Myr timescales, orders of magnitude larger than the usual Eddington limit.
7. The disk rapidly builds the BH from IMBH to SMBH masses, reaching $\gtrsim 2\times 10^6\,M_\odot$ in $\sim$1 Myr. Moreover, if pairing has occurred, the inner BH binary appears to undergo the expected process whereby the secondary accretes more rapidly until the two BHs are brought to

nearly equal mass, and they appear to grow at nearly identical rates, promoting nearly equal-mass BH–BH mergers.

This scenario therefore provides a natural explanation for the origins and rapid formation of high-redshift quasars in the early Universe. It also has critical implications for mergers of SMBHs in the LISA bands, and if the processes above can operate at even higher-mass scales ($\sim 10^9\,M_\odot$), it could also provide an explanation for the seemingly high rate of inferred SMBH mergers from pulsar timing (Agazie et al. 2023). We also note that we see a hypermagnetized, flux-frozen disk akin to those in Hopkins et al. (2024b) but under very different physical conditions and with distinct numerical methods and resolution and detailed physics treatments (as did, e.g., Gaburov et al. 2012), which suggests that these are robust and can indeed power super-Eddington mass accretion rates. It also demonstrates that one can quickly reach true SMBH masses without invoking exotic channels such as "direct collapse" (Volonteri & Rees 2005; Natarajan & Treister 2009; Mayer et al. 2010) of primordial gas clouds without fragmentation (indeed, here, fragmentation plays a key role in promoting rapid BH growth) or other "new physics" (Section 1).

In follow-up work, we hope to make more detailed observational predictions. But observations will be challenging, since we predict that this occurs on short time and small spatial scales in high-redshift systems, with comparable stellar and BH accretion bolometric luminosity, and the medium is still dusty and obscured at these times owing to the high gas densities. Still, it is immediately striking that the bolometric luminosities (~ 5–$50 \times 10^{44}\,\mathrm{erg\,s^{-1}}$, depending on the BH radiative efficiency), sizes ($\sim$10–100 pc), broadly comparable mix of stellar and active galactic nucleus luminosity, and colors (given the predicted dust column densities at large radii from Figure 4) this simulation would exhibit during its later evolution ($\gtrsim$0.7 Myr, after coalescence and disk formation) are all remarkably consistent with the observed properties of the unexpected population of "little red dots" seen by JWST at redshifts $z \sim 4$–10 (compare, e.g., Andika et al. 2024; Kocevski et al. 2024; Kokorev et al. 2024).

Interestingly, the BHs here end up well above the $M_{\rm BH}-M_*$ (bulge mass) but well below the $M_{\rm BH}-\sigma_*$ (velocity dispersion) correlations observed at $z=0$ (Kormendy & Ho 2013; McConnell & Ma 2013). This may therefore provide an explanation for apparently "overmassive" BHs observed at high redshift (and some low-redshift outliers; Seth et al. 2014; Trakhtenbrot et al. 2015; Walsh et al. 2016; Liepold et al. 2020) but also implies that typical systems must grow both in bulge mass and in BH mass before becoming "typical" $z=0$ massive classical bulges (as indeed predicted for more classical feedback-regulated models of the evolution of these properties; see Hopkins et al. 2008a, 2008b).

Of course, there are many caveats and limitations to the simulations here that merit further study. Our resolution is limited: future work with superresolution approaches like those in Anglés-Alcázar et al. (2021) would enable robust mapping of the behavior interior to the ROI and connection to GRMHD simulations like Kaaz et al. (2023) to horizon scales. Improving the star formation model with approaches like Grudić et al. (2021a) would free us from the universal IMF assumption and allow for actual predictions of exotic IMFs (and their effects) in high-redshift systems. In order to consider a "controlled" experiment, we utilize idealized initial conditions with preexisting gas and magnetic fields and BH seeds, which we could improve by following these systems in fully cosmological simulations with self-consistent seed BH formation models. And we consider only one simplified (and relatively "weak") model for "feedback" (in the form of jets, winds, and radiation) from BH accretion (motivated by the study in Shi et al. 2024 and slim disk models in Watarai et al. 2000 and Madau et al. 2014). But given that the hypermagnetized accretion disk here appears to be qualitatively, fundamentally distinct from the classical α-disks on which these feedback models are based, it is important to understand the horizon-scale (hence radiation, jet, and wind) properties of such disks in order to better inform next-generation subgrid feedback models.

Acknowledgments

Support for P.F.H. was provided by NSF research grants 20009234 and 2108318, NASA grant 80NSSC18K0562, and a Simons Investigator Award. Support for K.K. was provided by NASA through the NASA Hubble Fellowship grant HST-HF2-51510 awarded by the Space Telescope Science Institute, which is operated by the Association of Universities for Research in Astronomy, Inc., for NASA, under contract NAS5-26555. Numerical calculations were run on NSF/TACC allocation AST21010 and NASA HEC SMD-16-7592.

Data Availability

Simulation data involved in this work are available upon reasonable request to the authors.

ORCID iDs

Yanlong Shi https://orcid.org/0000-0002-0087-3237
Kyle Kremer https://orcid.org/0000-0002-4086-3180
Philip F. Hopkins https://orcid.org/0000-0003-3729-1684

References

Agazie, G., Anumarlapudi, A., Archibald, A. M., et al. 2023, ApJL, 951, L8
Andika, I. T., Jahnke, K., Onoue, M., et al. 2024, A&A, 685, A25
Anglés-Alcázar, D., Quataert, E., Hopkins, P. F., et al. 2021, ApJ, 917, 53
Bate, M. R., Bonnell, I. A., & Price, N. M. 1995, MNRAS, 277, 362
Begelman, M. C. 1979, MNRAS, 187, 237
Benincasa, S. M., Loebman, S. R., Wetzel, A., et al. 2020, MNRAS, 497, 3993
Blandford, R. D., & Begelman, M. C. 1999, MNRAS, 303, L1
Blandford, R. D., & Begelman, M. C. 2004, MNRAS, 349, 68
Bromm, V., & Loeb, A. 2003, ApJ, 596, 34
Bruel, T., Rodriguez, C. L., Lamberts, A., et al. 2023, A&A, 686, A106
Byrne, L., Faucher-Giguère, C.-A., Stern, J., et al. 2023, MNRAS, 520, 722
Chevance, M., Krumholz, M. R., McLeod, A. F., et al. 2023, in ASP Conf. Ser. 534, Protostars and Planets VII, ed. S. Inutsuka et al. (San Francisco, CA: ASP), 1
Crutcher, R. M. 2012, ARA&A, 50, 29
El-Badry, K., Rix, H.-W., Tian, H., Duchêne, G., & Moe, M. 2019, MNRAS, 489, 5822
Evstigneeva, E. A., Gregg, M. D., Drinkwater, M. J., & Hilker, M. 2007, AJ, 133, 1722
Fall, S. M., Krumholz, M. R., & Matzner, C. D. 2010, ApJL, 710, L142
Fan, X., Narayanan, V. K., Lupton, R. H., et al. 2001, AJ, 122, 2833
Gaburov, E., Johansen, A., & Levin, Y. 2012, ApJ, 758, 103
Geha, M., Guhathakurta, P., & van der Marel, R. P. 2002, AJ, 124, 3073
Goodman, J. 2003, MNRAS, 339, 937
Greene, J. E., Strader, J., & Ho, L. C. 2020, ARA&A, 58, 257
Grudić, M. Y., Boylan-Kolchin, M., Faucher-Giguère, C.-A., & Hopkins, P. F. 2020, MNRAS, 496, L127
Grudić, M. Y., Guszejnov, D., Hopkins, P. F., et al. 2018a, MNRAS, 481, 688

Grudić, M. Y., Guszejnov, D., Hopkins, P. F., Offner, S. S. R., & Faucher-Giguère, C.-A. 2021a, MNRAS, 506, 2199
Grudić, M. Y., Hafen, Z., Rodriguez, C. L., et al. 2023, MNRAS, 519, 1366
Grudić, M. Y., Hopkins, P. F., Faucher-Giguère, C.-A., et al. 2018b, MNRAS, 475, 3511
Grudić, M. Y., Hopkins, P. F., Quataert, E., & Murray, N. 2019, MNRAS, 483, 5548
Grudić, M. Y., Kruijssen, J. M. D., Faucher-Giguère, C.-A., et al. 2021b, MNRAS, 506, 3239
Guo, F., & Mathews, W. G. 2012, ApJ, 756, 181
Guo, F., & Oh, S. P. 2008, MNRAS, 384, 251
Guszejnov, D., Grudić, M. Y., Offner, S. S. R., et al. 2020, MNRAS, 492, 488
Guszejnov, D., Markey, C., Offner, S. S. R., et al. 2022, MNRAS, 515, 167
Haşegan, M., Jordán, A., Côté, P., et al. 2005, ApJ, 627, 203
Hopkins, P. F. 2015, MNRAS, 450, 53
Hopkins, P. F., Cox, T. J., Kereš, D., & Hernquist, L. 2008a, ApJS, 175, 390
Hopkins, P. F., Hernquist, L., Cox, T. J., & Kereš, D. 2008b, ApJS, 175, 356
Hopkins, P. F., Keres, D., Onorbe, J., et al. 2014, MNRAS, 445, 581
Hopkins, P. F., Murray, N., Quataert, E., & Thompson, T. A. 2010, MNRAS, 401, L19
Hopkins, P. F., Nadler, E. O., Grudić, M. Y., et al. 2023, MNRAS, 525, 5951
Hopkins, P. F., & Raives, M. J. 2016, MNRAS, 455, 51
Hopkins, P. F., Torrey, P., Faucher-Giguère, C.-A., Quataert, E., & Murray, N. 2016, MNRAS, 458, 816
Hopkins, P. F., Wellons, S., Anglés-Alcázar, D., Faucher-Giguère, C.-A., & Grudić, M. Y. 2022, MNRAS, 510, 630
Hopkins, P. F., Wetzel, A., Kereš, D., et al. 2018a, MNRAS, 477, 1578
Hopkins, P. F., Wetzel, A., Kereš, D., et al. 2018b, MNRAS, 480, 800
Hopkins, P. F., Grudic, M. Y., Su, K.-Y., et al. 2024a, OJAp, 7, 18
Hopkins, P. F., Squire, J., Su, K.-Y., et al. 2024b, OJAp, 7, 19
Hopkins, P. F., Squire, J., Quataert, E., et al. 2024c, OJAp, 7, 20
Inayoshi, K., Haiman, Z., & Ostriker, J. P. 2016, MNRAS, 459, 3738
Inayoshi, K., Visbal, E., & Haiman, Z. 2020, ARA&A, 58, 27
Izumi, T., Kawakatu, N., & Kohno, K. 2016, ApJ, 827, 81
Jiang, Y.-F., Stone, J. M., & Davis, S. W. 2014, ApJ, 796, 106
Jiang, Y.-F., Stone, J. M., & Davis, S. W. 2019, ApJ, 880, 67
Kaaz, N., Liska, M. T. P., Jacquemin-Ide, J., et al. 2023, ApJ, 955, 72
Keating, L. C., Richings, A. J., Murray, N., et al. 2020, MNRAS, 499, 837
Klessen, R. S. 2000, ApJ, 535, 869
Kocevski, D. D., Finkelstein, S. L., Barro, G., et al. 2024, arXiv:2404.03576
Kokorev, V., Caputi, K. I., Greene, J. E., et al. 2024, ApJ, 968, 38
Kormendy, J., & Ho, L. C. 2013, ARA&A, 51, 511
Kunz, M. W., & Mouschovias, T. C. 2009, ApJ, 693, 1895
Lai, D., & Muñoz, D. J. 2023, ARA&A, 61, 517
Li, H., Vogelsberger, M., Marinacci, F., & Gnedin, O. Y. 2019, MNRAS, 487, 364
Liepold, C. M., Quenneville, M. E., Ma, C.-P., et al. 2020, ApJ, 891, 4
Ma, L., Hopkins, P. F., Ma, X., et al. 2021, MNRAS, 508, 1973
Ma, X., Hopkins, P. F., Boylan-Kolchin, M., et al. 2018, MNRAS, 477, 219
Ma, X., Grudić, M. Y., Quataert, E., et al. 2020, MNRAS, 493, 4315
Mac Low, M.-M., & Klessen, R. S. 2004, RvMP, 76, 125
Madau, P., Haardt, F., & Dotti, M. 2014, ApJL, 784, L38
Mayer, L., Kazantzidis, S., Escala, A., & Callegari, S. 2010, Natur, 466, 1082
McConnell, N. J., & Ma, C.-P. 2013, ApJ, 764, 184
McKee, C. F., & Ostriker, E. C. 2007, ARA&A, 45, 565
Natarajan, P., & Treister, E. 2009, MNRAS, 393, 838
Orr, M. E., Hayward, C. C., Hopkins, P. F., et al. 2018, MNRAS, 478, 3653
Orr, M. E., Hayward, C. C., Medling, A. M., et al. 2020, MNRAS, 496, 1620
Orr, M. E., Hatchfield, H. P., Battersby, C., et al. 2021, ApJL, 908, L31
Ponnada, S. B., Panopoulou, G. V., Butsky, I. S., et al. 2022, MNRAS, 516, 4417
Portegies Zwart, S. F., Baumgardt, H., Hut, P., Makino, J., & McMillan, S. L. W. 2004, Natur, 428, 724
Rantala, A., Naab, T., & Lahén, N. 2024, MNRAS, 531, 3770
Rodriguez, C. L., Hafen, Z., Grudić, M. Y., et al. 2023, MNRAS, 521, 124
Scoville, N., Murchikova, L., Walter, F., et al. 2017, ApJ, 836, 66
Seth, A. C., van den Bosch, R., Mieske, S., et al. 2014, Natur, 513, 398
Shakura, N. I., & Sunyaev, R. A. 1973, A&A, 24, 337
Shen, X., Hopkins, P. F., Faucher-Giguère, C.-A., et al. 2020, MNRAS, 495, 3252
Shi, Y., Grudić, M. Y., & Hopkins, P. F. 2021, MNRAS, 505, 2753
Shi, Y., Kremer, K., Grudić, M. Y., Gerling-Dunsmore, H. J., & Hopkins, P. F. 2023, MNRAS, 518, 3606
Shi, Y., Kremer, K., & Hopkins, P. F. 2024, arXiv:2405.12164
Silk, J., & Rees, M. J. 1998, A&A, 331, L1
Sądowski, A., Narayan, R., Tchekhovskoy, A., et al. 2015, MNRAS, 447, 49
Su, K.-Y., Hopkins, P. F., Bryan, G. L., et al. 2021, MNRAS, 507, 175
Swinbank, A. M., Smail, I., Sobral, D., et al. 2012, ApJ, 760, 130
Tacconi, L. J., Genzel, R., Saintonge, A., et al. 2018, ApJ, 853, 179
Torrey, P., Hopkins, P. F., Faucher-Giguère, C.-A., et al. 2020, MNRAS, 497, 5292
Trakhtenbrot, B., Urry, C. M., Civano, F., et al. 2015, Sci, 349, 168
Volonteri, M., Habouzit, M., & Colpi, M. 2021, NatRP, 3, 732
Volonteri, M., & Rees, M. J. 2005, ApJ, 633, 624
Wada, K., Papadopoulos, P. P., & Spaans, M. 2009, ApJ, 702, 63
Walcher, C. J., van der Marel, R. P., McLaughlin, D., et al. 2005, ApJ, 618, 237
Walsh, J. L., van den Bosch, R. C. E., Gebhardt, K., et al. 2016, ApJ, 817, 2
Wang, F., Yang, J., Fan, X., et al. 2021, ApJL, 907, L1
Watarai, K.-y., Fukue, J., Takeuchi, M., & Mineshige, S. 2000, PASJ, 52, 133
Xiao, H., Shen, X., Hopkins, P. F., & Zurek, K. M. 2021, JCAP, 2021, 039
Yang, J., Wang, F., Fan, X., et al. 2020, ApJL, 897, L14
Yu, Q., & Tremaine, S. 2002, MNRAS, 335, 965
Zweibel, E. G. 2017, PhPl, 24, 055402